

RUP-18-15

PBH abundance from random Gaussian curvature perturbations and a local density threshold

Chul-Moon Yoo,^{1,*} Tomohiro Harada,^{2,†} Jaume Garriga,^{3,‡} and Kazunori Kohri^{4,5,6,§}

¹*Division of Particle and Astrophysical Science,
Graduate School of Science, Nagoya University, Nagoya 464-8602, Japan*

² *Department of Physics, Rikkyo University, Toshima, Tokyo 171-8501, Japan*

³*Departament de Física Quàntica i Astrofísica,
Institut de Ciències del Cosmos, Universitat de Barcelona,
Martí i Franquès 1, 08028 Barcelona, Spain*

⁴*Rudolf Peierls Centre for Theoretical Physics,
The University of Oxford, 1 Keble Road, Oxford, OX1 3NP, UK*

⁵*Institute of Particle and Nuclear Studies, KEK,
1-1 Oho, Tsukuba, Ibaraki 305-0801, Japan*

⁶*The Graduate University for Advanced Studies (SOKENDAI),
1-1 Oho, Tsukuba, Ibaraki 305-0801, Japan*

The production rate of primordial black holes is often calculated by considering a nearly Gaussian distribution of cosmological perturbations, and assuming that black holes will form in regions where the amplitude of such perturbations exceeds a certain threshold. A threshold ζ_{th} for the curvature perturbation is somewhat inappropriate for this purpose, because it depends significantly on environmental effects, not essential to the local dynamics. By contrast, a threshold δ_{th} for the density perturbation at horizon crossing seems to provide a more robust criterion. On the other hand, the density perturbation is known to be bounded above by a maximum limit δ_{max} , and given that δ_{th} is comparable to δ_{max} , the density perturbation will be far from Gaussian near or above the threshold. In this paper we provide a new plausible estimate for the primordial black hole abundance based on peak theory. In our approach, we assume a Gaussian distribution for the curvature perturbation, while an optimized criterion for PBH formation is imposed, based on the locally averaged density perturbation around the nearly spherically symmetric high peaks. Both variables are related by the full nonlinear expression derived in the long-wavelength approximation of general relativity. We find that the mass spectrum is shifted to larger mass scales by one order of magnitude or so, compared to a conventional calculation. The abundance of PBHs becomes significantly larger than the conventional one, by many orders of magnitude, mainly due to the optimized criterion for PBH formation.

* yoo@gravity.phys.nagoya-u.ac.jp

† harada@rikkyo.ac.jp

‡ jaume.garriga@ub.edu

§ kohri@post.kek.jp

I. INTRODUCTION

Processes which may lead to the formation of primordial black holes (PBHs), along with their cosmological implications, have been extensively investigated in the literature since the pioneering work of Zel'dovich and Novikov [1] and Hawking [2]. PBHs may be produced by gravitational collapse in regions with a large amplitude of density perturbations in the early Universe, and measurements or constraints on their abundance can be regarded as a probe of the primordial spectrum and the underlying inflationary model. The latest observational constraints are summarized in, e.g. Refs. [3, 4]. So far, PBHs have been actively studied as candidates of dark matter (e.g., see Refs. [4–15] and references therein). In addition, the recent discovery of gravitational waves emitted from binary black holes (BBHs) [16, 17] has stimulated the investigation of PBH binaries and their merger rates [18–21].

In this paper, we will focus on the formation of PBHs in the radiation dominated era (see Refs. [22–24] for cases of the matter dominated era), due to some enhanced feature in the primordial power spectrum of density perturbations around some specific scale.¹ A rough criterion for the formation of PBHs was first proposed by Carr [6], and much numerical work has been done in search of a more accurate criterion [28–37]. The perturbation variables which are used to characterize the amplitude of the initial inhomogeneity are roughly divided into two sorts: the density perturbation, and the curvature perturbation. For instance, Shibata and Sasaki [30] discussed the threshold for PBH formation by using the curvature variable which is given by the conformal factor of the spatial metric. On the other hand, in Refs. [32–37], the threshold value is given for the averaged density perturbation at the horizon entry in the comoving slicing, and in the lowest order long-wavelength expansion. The threshold value of the density perturbation is given by $\delta_{\text{th}} \approx 0.42 - 0.66$ depending on the perturbation profile. The lowest threshold value seems to correspond to the value analytically derived in Ref. [38] with significant simplification.

As for the curvature variable, it has been suggested in Ref. [39] that the threshold is strongly affected by environmental effects, while that of a density perturbation is not. This fact has been also numerically demonstrated in Ref. [40]. One extreme example which shows the significance of the environmental effects is the estimate of the threshold of the curvature perturbation suggested in Ref. [38]. There, an (irrelevant) extremely low value of $\zeta_{\text{th}} \simeq 0.0862$ is obtained, due to the existence of an unphysical negative density region in the environment in the specific model adopted there. However, even if we keep the positivity of the density in the environment, the threshold value of the curvature perturbation can be significantly affected [40]. This can be intuitively understood if we consider the curvature perturbation as the general relativistic counterpart of the Newtonian potential, which can be shifted by an arbitrary constant. Since, at least in spherically symmetric systems, the process of PBH formation can be described in a quasi-local manner, the use of a threshold value for a quasi-local perturbation variable seems to be more appropriate (see Sec. VII and VIII in Ref. [40] for details).

¹ Inflation can also produce relics, such as vacuum bubbles and domain walls with a distribution of sizes, which may in turn produce PBH during the subsequent radiation dominated era (see e.g. [25–27] and references therein). In this case, the relics behave as active seeds, and trigger gravitational collapse with unit probability if their initial comoving size is sufficiently large. Our present considerations do not apply to such situation.

A useful criterion has been proposed in Ref. [30] for spherically symmetric systems based on the so-called compaction function, which is equivalent to one half of the volume average of the density perturbation δ at the time of horizon entry [40]. The criterion for PBH formation is that the maximum value of the compaction function as a function of the averaging radius lies above a specified threshold $\mathcal{C}_{\text{th}} = \delta_{\text{th}}/2$, at the time when the averaging radius enters the horizon. Such threshold value has been found to be quite robust. This has been tested by considering two different families of profiles for the perturbation, and a broad range of parameters [40]. In what follows, we will not further discuss the possible profile dependence of the threshold, but simply assume the existence of a typical value. We also note that, although our framework is applicable to generic non-spherical systems, we will adopt a criterion for PBH formation by referring to the compaction function in the corresponding spherical system. This is justified because high peaks of a random Gaussian field tend to be spherical.

The main purpose of this paper is to find an estimate for the abundance of PBHs once a threshold value of the averaged density perturbation is provided. One conventional way is to apply the Press-Schechter(PS) formalism to the density perturbation by assuming that this variable is Gaussian distributed. However, due to the local dynamics of overdense regions, there is an upper limit for the value of the density perturbation at horizon crossing. This was first observed in Refs. [38, 41], in the context of a simplified “3 zone model” where a spherical homogeneous overdensity is embedded in a flat Friedmann-Lemaître-Robertson-Walker(FLRW) environment. More generally, it was found [40] that for spherically symmetric perturbations with any profile, the maximum density perturbation at horizon crossing in the co-moving slicing is bounded by $\delta_{\text{max}} \approx 2/3$. The argument will be reviewed in Section II.² Noting that δ_{th} is in fact comparable to the maximum value δ_{max} (above which the probability distribution should vanish) a naive application of the Gaussian distribution seems rather questionable. In addition, while the threshold is often set for the density perturbation, the statistical properties of the primordial curvature perturbation are usually better understood. Therefore, it is natural to consider the abundance of PBHs by combining the threshold of the density perturbation with the statistical properties of the curvature perturbation. Since PBH formation is a non-linear process, a non-linear relation between these perturbation variables should be taken into account. In this paper, we address the calculation of the PBH abundance by using the peak theory for the Gaussian probability distribution of the curvature perturbation, and the non-linear relation between curvature and density perturbation in the long-wavelength limit. Readers not interested in the details of the derivation can skip directly to Eq. (65), and the ensuing explanation on how to use it.

The plan of the paper is the following. In Section II we discuss the perturbation variables and the implementation of a threshold for PBH formation. In Section III we consider the statistical properties of the Taylor expansion coefficients of the Gaussian random field ζ

² In Ref. [41] the maximum density perturbation at horizon crossing in the geodesic slicing is found to be $\delta_{\text{max}}^G = 9/16$. In the long wavelength approximation [40], such value translates into the comoving slicing as $\delta_{\text{max}} \approx 3/4$. Note that this differs from the determination given in [38, 40] by a factor of $8/9$, which may be related to the extrapolation of the long wavelength approximation in relating the different gauges at horizon crossing.

around a given point. In Section IV, where we discuss the probability for PBH formation, based on peak theory and on our implementation of the threshold on the averaged density perturbation. The results will be compared to the more conventional PS approach. Our conclusions are summarized in Section V. Some technical aspects are discussed in the Appendices. Throughout this paper, we use the geometrized units in which both the speed of light and Newton's gravitational constant are unity, $c = G = 1$.

II. PERTURBATION VARIABLES AND THRESHOLD FOR PBH FORMATION

A. perturbation variables

We will be interested in the density perturbation in the comoving slicing, which is orthogonal to the fluid world line. In the long-wavelength approximation, the curvature perturbation ζ and the density perturbation δ with the comoving slicing are related by [40],

$$\delta = -\frac{4(1+w)}{3w+5} \frac{1}{a^2 H^2} e^{5/2\zeta} \Delta (e^{-\zeta/2}), \quad (1)$$

where w is the equation of state parameter, a is the scale factor, H is the Hubble rate, Δ is the Laplacian of the reference flat metric, and the spatial metric is given by

$$ds_3^2 = a^2 e^{-2\zeta} \tilde{\gamma}_{ij} dx^i dx^j, \quad (2)$$

with $\det \tilde{\gamma}$ being the same as the determinant of the reference flat metric. Since the density perturbation can be expressed by using the value of ζ and its derivatives up to the second order, it will be useful for our purposes to consider the Taylor expansion of the field $\zeta(x_i)$:

$$\zeta = \zeta_0 + \zeta_1^i x_i + \frac{1}{2} \zeta_2^{ij} x_i x_j + \mathcal{O}(x^3). \quad (3)$$

The density perturbation around an extremum point $\zeta_1^i = 0$ is given by

$$\delta_{\text{ext}} = \frac{4}{9} \frac{1}{a^2 H^2} e^{2\zeta_0} \zeta_2, \quad (4)$$

where

$$\zeta_2 := \Delta \zeta|_{\mathbf{x}=\mathbf{0}} = \zeta_2^{11} + \zeta_2^{22} + \zeta_2^{33}, \quad (5)$$

(see Appendix A for an estimate of the typical separation between the peaks of ζ and δ) and we have used $w = 1/3$, since we will be considering a radiation fluid in this paper. Expressing ζ_2 in terms of an amplitude μ and a spatial scale $1/k_*$, as

$$\zeta_2 = \mu k_*^2,$$

we obtain

$$\delta_{\text{ext}} = \frac{4}{9} e^{2\zeta_0} \frac{k_*^2}{a^2 H^2} \mu. \quad (6)$$

Since ζ_0 gives the zero mode for the curvature perturbation, it can be absorbed by a renormalized scale factor \bar{a} , defined by

$$\bar{a} := a e^{-\zeta_0}. \quad (7)$$

Then, we obtain

$$\delta_{\text{ext}} = \frac{4}{9} \frac{k_*^2}{\bar{a}^2 H^2} \mu. \quad (8)$$

In order to extract the spatial scale $1/k_*$, we use the value ζ_4 defined by

$$\zeta_4 := \Delta \Delta \zeta|_{\mathbf{x}=0}. \quad (9)$$

That is, in terms of ζ_2 and ζ_4 , the variables μ and k_* are given by³

$$k_*^2 = -\frac{\zeta_4}{\zeta_2}, \quad (10)$$

$$\mu = -\frac{\zeta_2^2}{\zeta_4}. \quad (11)$$

In this paper we assume that ζ is a Gaussian random field, and therefore the distribution of the variables ζ_2 and ζ_4 is Gaussian. On the other hand, the threshold for PBH formation will be expressed in terms of the variable μ , as we will now discuss.

B. PBH formation criterion for spherical systems

We will be interested mainly in high peaks, which tend to be nearly spherically symmetric [42]. Therefore, in this Subsection, we propose a criterion for PBH formation assuming spherical symmetry. Here, we basically follow and refer to the discussions and calculation in Ref. [40].

First, let us define the compaction function \mathcal{C} as

$$\mathcal{C} := \frac{\delta M}{R}, \quad (12)$$

where R is the areal radius at the radius r , and δM is the excess of the Misner-Sharp mass M_{MS} enclosed by the sphere of the radius r compared with the mass M_{F} inside the sphere in the fiducial flat FLRW universe with the same areal radius. From Eqs. (5.9), (5.26), (5.27)

³ Another possible definition for the inverse length-scale of the perturbation would be $\bar{k}_*^2 = -\zeta_2/\zeta_0$. Actually, by using this definition and following a calculation similar to the one presented in the text, a simpler expression for the fraction of PBHs can be found. However, this treatment gives a qualitatively different result. In this paper, we do not adopt \bar{k}_* as a typical lengthscale for the following two reasons. First, the use of ζ_0 to define the physical scale seems counter-intuitive, given that a constant shift in ζ is physically irrelevant. The other reason is from an analogy with the simple three zone model described in [38]. If we do not have any information about the profile of the density perturbation beyond second order in the Taylor expansion of ζ , the situation is similar to the three zone model, where the scale of the inhomogeneity (i.e. the comoving radius of the over-dense region) must be fixed by hand. This suggests that we need additional information about the scale of the inhomogeneity, which in the present case can be obtained from ζ_4 .

and (5.28) in Ref. [40], we find the following expressions for each variable:

$$M_{\text{MS}}(r) = \frac{3}{2}H^2 \int_0^r dx x^2 (1 + \delta) e^{-3\zeta} (1 - r\zeta'), \quad (13)$$

$$M_{\text{F}}(r) = \frac{1}{2}H^2 a^3 r^3, \quad (14)$$

$$\mathcal{C}(r) = \frac{M_{\text{MS}}(r) - M_{\text{F}}(r e^{-\zeta})}{a r e^{-\zeta}}. \quad (15)$$

In the limit of the long-wavelength approximation, for any gauge, the compaction function is given by:

$$\mathcal{C} = \frac{1}{2}\bar{\delta}(HR)^2, \quad (16)$$

where $\bar{\delta}$ is the volume average of the density perturbation δ within the radius r (see Eq. (5.31) in Ref. [40]). From the definition of \mathcal{C} , we can derive the following simple form in the comoving slicing (see also Eq. (6.33) in Ref. [40]):

$$\mathcal{C}(r) = \frac{1}{3} \left[1 - (1 - r\zeta')^2 \right] = \frac{1}{3} \left[1 - \frac{e^{2\zeta}}{a^2} R'^2 \right]. \quad (17)$$

From this expression, it is clear that $\mathcal{C} \leq 1/3$. If we identify the time of horizon entry of the perturbation from the condition $HR = 1$, then, from Eq. (16), the corresponding averaged density perturbation is $\bar{\delta} < \delta_{\text{max}} = 2/3$, as discussed in the introduction. The existence of the region $R' < 0$ corresponds to the Type II PBH formation reported in Ref. [41]. In what follows, we focus on the Type I cases, that is, $R' > 0$.

We will also assume that the function \mathcal{C} is a smooth function of r for $r > 0$. Then, the value of \mathcal{C} takes the maximum value \mathcal{C}^{max} at r_m which satisfies⁴

$$\mathcal{C}'(r_m) = 0 \Leftrightarrow (\zeta' + r\zeta'')|_{r=r_m} = 0. \quad (18)$$

We consider the following criterion for PBH formation:

$$\mathcal{C}^{\text{max}} > \mathcal{C}_{\text{th}} \equiv \frac{1}{2}\delta_{\text{th}}. \quad (19)$$

In the constant-mean-curvature(CMC) slice, the threshold $\mathcal{C}_{\text{th}}^{\text{CMC}}$ for PBH formation is evaluated as $\simeq 0.4 \pm 0.03$ (see Figs. 2 and 3 or TABLE I and II in Ref. [40]). This threshold corresponds to the perturbation profiles of Refs. [30, 33, 34], and is found to be quite robust for a broad range of parameters. Since the relation between the density perturbation in the comoving slice (δ) and the CMC slice (δ_{CMC}) is given by

$$\delta = \frac{2}{3}\delta_{\text{CMC}}, \quad (20)$$

the threshold value in the comoving slice is given by $\mathcal{C}_{\text{th}} \simeq 0.267$ which corresponds to $\delta_{\text{th}} \simeq 0.533$. In this paper we shall use this as a reference value. We should keep in mind,

⁴ We acknowledge that I. Musco has pointed out the importance of the radius r_m to us[43].

however, that the threshold value is not completely independent of profile. For instance, as mentioned in the introduction, the threshold in a 3-zone model with a homogeneous overdensity the threshold is somewhat lower.

In order to evaluate the value of r_m , we need to consider the profile of the inhomogeneity. It can be shown that even if we fix the value of ζ_2 and ζ_4 by using k_* and μ through Eqs. (10) and (11), the value of r_m can change about 30% depending on the higher order coefficients of the Taylor expansion. This issue is discussed in Appendix C. Hence, for the moment, we keep the expressions as generic as possible. Let us consider the following functional form:

$$\zeta - \zeta_0 = \mu g(k_* r). \quad (21)$$

We assume that $g(k_* r)$ satisfies the following conditions:

$$\begin{aligned} \left. \frac{dg(k_* r)}{dr} \right|_{r=0} &= 0, & \left. \frac{d^2 g(k_* r)}{dr^2} \right|_{r=0} &= \frac{1}{3} \frac{\zeta_2}{\mu} = \frac{1}{3} k_*^2, \\ \left. \frac{d^3 g(k_* r)}{dr^3} \right|_{r=0} &= 0, & \left. \frac{d^4 g(k_* r)}{dr^4} \right|_{r=0} &= \frac{1}{5} \frac{\zeta_4}{\mu} = -\frac{1}{5} k_*^4 \end{aligned} \quad (22)$$

so that it can be compatible with Eqs. (10) and (11). Then, Eq. (18) can be rewritten as

$$g'(\ell) + \ell g''(\ell) = 0, \quad (23)$$

where we have defined ℓ as

$$\ell := k_* r_m. \quad (24)$$

The value of \mathcal{C}^{\max} can be expressed as

$$\mathcal{C}^{\max} = -\frac{1}{3} \ell^2 g'(\ell)^2 \mu^2 + \frac{2}{3} \ell g'(\ell) \mu. \quad (25)$$

The threshold value follows from the condition $\mathcal{C}^{\max}(\mu_{\text{th}}) = \delta_{\text{th}}/2$. This is a quadratic equation for μ_{th} which gives

$$\mu_{\text{th}} = \frac{1}{2\ell g'(\ell)} \left(2 - \sqrt{4 - 6\delta_{\text{th}}} \right), \quad (26)$$

where the smaller root has been chosen. For any given functional form of g , we consider that a PBH is formed if the amplitude μ is larger than μ_{th} .

In Eq. (19), we have implicitly used Eq. (16) with the horizon entry condition $R(r_m) = ar_m e^{-\zeta(r_m)} = 1/H$. This can be rewritten as

$$\bar{a}H = \frac{k_*}{\ell} e^{\mu g(\ell)}. \quad (27)$$

We note that this coincides with the condition $2M_F(r_m e^{-\zeta(r_m)}) = H^{-1}$, or with the long-wavelength limit of the condition $2M_{\text{MS}}(r_m) = H^{-1}$.

In what follows we will treat μ and k_* as random variables, but the higher order coefficients of the Taylor expansion as fixed variables for simplicity. In principle, these should be treated as new variables, and we leave the general treatment of a random profile for further research.

Meanwhile, we note that for the case of a monochromatic spectrum, the profile of a spherical perturbation is unambiguously determined to be of the form $g(k_*r) = 1 - \text{sinc}(k_*r)$. This will suffice to understand the effect the non-linear relations which we are investigating on the PBH abundance. For comparison, some plausible alternative profiles are considered in Appendix C.

III. RANDOM GAUSSIAN DISTRIBUTION OF ζ

A key assumption is the random Gaussian distribution of ζ with its power spectrum $\mathcal{P}(k)$ defined by the following equation:

$$\langle \tilde{\zeta}^*(\mathbf{k}) \tilde{\zeta}(\mathbf{k}') \rangle = \frac{2\pi^2}{k^3} \mathcal{P}(k) (2\pi)^3 \delta(\mathbf{k} - \mathbf{k}'), \quad (28)$$

where $\tilde{\zeta}(\mathbf{k})$ is the Fourier transform of ζ and the bracket $\langle \dots \rangle$ denotes the ensemble average. In this section, we briefly review Ref. [42] to introduce the probability distribution for the curvature variables. Due to the random Gaussian assumption, the probability distribution of any set of linear combination of the variable $\zeta(x_i)$ is given by a multi-dimensional Gaussian probability distribution [42, 44]:

$$P(V_I) d^n V_I = (2\pi)^{-n/2} |\det \mathcal{M}|^{-1/2} \exp \left[-\frac{1}{2} V_I (\mathcal{M}^{-1})^{IJ} V_J \right] d^n V, \quad (29)$$

where the components of the matrix \mathcal{M} are given by the correlation $\langle V_I V_J \rangle$ defined by

$$\langle V_I V_J \rangle := \int \frac{d\mathbf{k}}{(2\pi)^3} \frac{d\mathbf{k}'}{(2\pi)^3} \langle \tilde{V}_I^*(\mathbf{k}) \tilde{V}_J(\mathbf{k}') \rangle \quad (30)$$

with $\tilde{V}_I(\mathbf{k}) = \int d^3x V_I(\mathbf{x}) e^{i\mathbf{k}\mathbf{x}}$.

The non-zero correlations between two of ζ_0 , ζ_1^i and ζ_2^{ii} are given by

$$\langle \zeta_0 \zeta_0 \rangle = \sigma_0^2, \quad (31)$$

$$-3 \langle \zeta_0 \zeta_2^{ii} \rangle = 3 \langle \zeta_1^i \zeta_1^i \rangle = \sigma_1^2, \quad (32)$$

$$5 \langle \zeta_2^{ii} \zeta_2^{ii} \rangle = 15 \langle \zeta_2^{ii} \zeta_2^{jj} \rangle = 15 \langle \zeta_2^{ij} \zeta_2^{ij} \rangle = \sigma_2^2 \text{ with } i \neq j, \quad (33)$$

where σ_n are the moments defined by

$$\sigma_n^2 := \int \frac{dk}{k} k^{2n} \mathcal{P}(k) \quad (34)$$

with n being a non-negative integer. In practice, when we calculate the moments, we will multiply the integrand by the square of a window function which has a typical scale k_* . However, for the time being, we treat the moments as constants. The scale dependence will be introduced in Sec. IV A, and the ambiguity in the choice of the window function will be discussed in Sec. IV D.

Let us focus on the variables ζ_2^{ij} . There are 6 independent variables $\zeta_2^A := (\zeta_2^{11}, \zeta_2^{22}, \zeta_2^{33}, \zeta_2^{12}, \zeta_2^{23}, \zeta_2^{31})$. It can be shown that, taking the principal direction of the matrix ζ_2^{ij} , the volume element can be rewritten as follows:

$$\prod_{A=1}^6 d\zeta_2^A = (\lambda_1 - \lambda_2)(\lambda_2 - \lambda_3)(\lambda_1 - \lambda_3) \sin \theta_1 d\lambda_1 d\lambda_2 d\lambda_3 d\theta_1 d\theta_2 d\theta_3, \quad (35)$$

where λ_i are eigen values of the matrix ζ_2^{ij} with $\lambda_1 \geq \lambda_2 \geq \lambda_3$ and θ_i are the Euler angles to take the principal direction. From the integration with respect to the Euler angles, the factor $2\pi^2$ arises.

Following Ref. [42], we introduce new variables ν , η_i and ξ_i as follows:

$$\nu = -\zeta_0/\sigma_0, \quad (36)$$

$$\eta_i = \zeta_1^i/\sigma_1, \quad (37)$$

$$\xi_1 = (\lambda_1 + \lambda_2 + \lambda_3)/\sigma_2, \quad (38)$$

$$\xi_2 = \frac{1}{2}(\lambda_1 - \lambda_3)/\sigma_2, \quad (39)$$

$$\xi_3 = \frac{1}{2}(\lambda_1 - 2\lambda_2 + \lambda_3)/\sigma_2. \quad (40)$$

λ_i is described in terms of ξ_i as follows:

$$\lambda_1 = \frac{1}{3}(\xi_1 + 3\xi_2 + \xi_3)\sigma_2, \quad (41)$$

$$\lambda_2 = \frac{1}{3}(\xi_1 - 2\xi_3)\sigma_2, \quad (42)$$

$$\lambda_3 = \frac{1}{3}(\xi_1 - 3\xi_2 + \xi_3)\sigma_2. \quad (43)$$

Then, the probability distribution can be expressed as

$$P(\nu, \boldsymbol{\xi}, \boldsymbol{\eta}) d\nu d\boldsymbol{\xi} d\boldsymbol{\eta} = P_1(\nu, \xi_1) P_2(\xi_2, \xi_3, \boldsymbol{\eta}) d\nu d\boldsymbol{\xi} d\boldsymbol{\eta}, \quad (44)$$

where

$$P_1(\nu, \xi_1) d\nu d\xi_1 = \frac{1}{2\pi} \frac{1}{\sqrt{1 - \gamma_1^2}} \exp \left[-\frac{1}{2} \left\{ \frac{(\nu - \gamma_1 \xi_1)^2}{1 - \gamma_1^2} + \xi_1^2 \right\} \right] d\nu d\xi_1 \quad (45)$$

and

$$\begin{aligned} P_2(\boldsymbol{\eta}, \xi_2, \xi_3) d\xi_2 d\xi_3 d\boldsymbol{\eta} &= \frac{5^{5/2} 3^{7/2}}{(2\pi)^2} \xi_2 (\xi_2^2 - \xi_3^2) \exp \left[-\frac{5}{2} \left\{ 3\xi_2^2 + \xi_3^2 \right\} \right] \\ &\times \exp \left[-\frac{3}{2} \left\{ \eta_1^2 + \eta_2^2 + \eta_3^2 \right\} \right] d\xi_2 d\xi_3 d\boldsymbol{\eta} \end{aligned} \quad (46)$$

with

$$\gamma_1 = \sigma_1^2/(\sigma_0 \sigma_2), \quad (47)$$

$\xi_2 \geq \xi_3 \geq -\xi_2$ and $\xi_2 \geq 0$. We have abbreviated the three components variables ξ_i and η_i as $\boldsymbol{\xi}$ and $\boldsymbol{\eta}$.

So far, we have considered the Taylor expansion of ζ up to the second order. Here, let us introduce another coefficient ζ_4 . Introducing a new variable $\omega := -\zeta_4/\sigma_4$, we obtain the following non-zero correlations:

$$\begin{aligned} <\omega\omega> &= 1, \\ <\nu\omega> &= \gamma_2 := \sigma_2^2/(\sigma_0\sigma_4), \\ <\xi_1\omega> &= \gamma_3 := \sigma_3^2/(\sigma_2\sigma_4). \end{aligned} \quad (48)$$

Adding the new variable ω , we modify the probability distribution function P_1 to have three independent variables ν , ξ_1 and ω as follows:

$$\begin{aligned} P_1(\nu, \xi_1, \omega) d\nu d\xi_1 d\omega &= (2\pi)^{-3/2} |D|^{-1/2} \exp \left[-\frac{1}{2D} \left\{ (1 - \gamma_3^2)\nu^2 + (1 - \gamma_2^2)\xi_1^2 + (1 - \gamma_1^2)\omega^2 \right. \right. \\ &\quad \left. \left. - 2(\gamma_1 - \gamma_2\gamma_3)\nu\xi_1 - 2(\gamma_2 - \gamma_3\gamma_1)\omega\nu - 2(\gamma_3 - \gamma_1\gamma_2)\xi_1\omega \right\} \right] d\nu d\xi_1 d\omega, \end{aligned} \quad (49)$$

where

$$D = \det \mathcal{M}_1 = 1 - \gamma_1^2 - \gamma_2^2 - \gamma_3^2 + 2\gamma_1\gamma_2\gamma_3 \quad (50)$$

with

$$\mathcal{M}_1 = \begin{pmatrix} 1 & \gamma_1 & \gamma_2 \\ \gamma_1 & 1 & \gamma_3 \\ \gamma_2 & \gamma_3 & 1 \end{pmatrix}. \quad (51)$$

IV. PBH FRACTION TO THE TOTAL DENSITY

A. General expression

Following Ref. [42], we start by deriving an expression for the peak number density. The probability distribution can be written as

$$P(\nu, \boldsymbol{\eta}, \boldsymbol{\xi}, \omega) d\nu d\boldsymbol{\eta} d\boldsymbol{\xi} d\omega = P_1(\nu, \xi_1, \omega) d\nu d\xi_1 d\omega P_2(\boldsymbol{\eta}, \xi_2, \xi_3) d\boldsymbol{\eta} d\xi_2 d\xi_3. \quad (52)$$

Let us focus on the parameters ν , $\boldsymbol{\xi}$ and ω to characterize each extremum. We define $n_{\text{ext}}(\mathbf{x}, \nu, \xi_1, \omega)$ as the distribution of extrema of the field ζ in the space of $(\mathbf{x}, \nu, \xi_1, \omega)$, that is,

$$n_{\text{ext}}(\mathbf{x}, \nu, \xi_1, \omega) \Delta \mathbf{x} \Delta \nu \Delta \xi_1 \Delta \omega = \text{number of extrema in the volume } \Delta \mathbf{x} \Delta \nu \Delta \xi_1 \Delta \omega. \quad (53)$$

Then, $n_{\text{ext}}(\mathbf{x}, \nu, \xi_1, \omega)$ can be expressed as follows:

$$n_{\text{ext}}(\mathbf{x}, \nu, \xi_1, \omega) d\mathbf{x} d\nu d\xi_1 d\omega = \sum_p \delta(\mathbf{x} - \mathbf{x}_p) \delta(\nu - \nu_p) \delta(\xi_1 - \xi_{1p}) \delta(\omega - \omega_p) d\mathbf{x} d\nu d\xi_1 d\omega, \quad (54)$$

where the label p denotes variables of each extremum. Then, \mathbf{x}_p is the position of the extremum, that is, $\zeta_1 = \boldsymbol{\eta} = 0$ at $\mathbf{x} = \mathbf{x}_p$. Therefore, we obtain

$$\delta(\mathbf{x} - \mathbf{x}_p) = \det \left| \frac{\partial^2 \zeta}{\partial x^i \partial x^j} \right|_{\mathbf{x}=\mathbf{x}_p} \delta(\zeta_1) = \sigma_1^{-3} |\lambda_1 \lambda_2 \lambda_3| \delta(\boldsymbol{\eta}), \quad (55)$$

where

$$\lambda_1 \lambda_2 \lambda_3 = \frac{1}{27} ((\xi_1 + \xi_3)^2 - 9\xi_2^2) (\xi_1 - 2\xi_3) \sigma_2^3. \quad (56)$$

The peak number density $n_{\text{pk}}(\nu, \xi_1, \omega)$ is given by the ensemble average of $n_{\text{ext}} \Theta(\lambda_3) \Theta(\omega)$ as follows:

$$\begin{aligned} n_{\text{pk}}(\nu, \xi_1, \omega) d\nu d\xi_1 d\omega &= \langle n_{\text{ext}} \Theta(\lambda_3) \Theta(\omega) \rangle d\nu d\xi_1 d\omega \\ &= \sigma_1^{-3} \left[\int d\nu_p d\xi_{1p} d\omega_p d\boldsymbol{\eta} d\boldsymbol{\xi} \left\{ P(\nu_p, \boldsymbol{\eta}, \xi_{1p}, \xi_2, \xi_3, \omega) |\lambda_1 \lambda_2 \lambda_3| \right. \right. \\ &\quad \left. \left. \delta(\boldsymbol{\eta}) \delta(\nu - \nu_p) \delta(\xi_1 - \xi_{1p}) \delta(\omega - \omega_p) \Theta(\lambda_3) \Theta(\omega) \right\} \right] d\nu d\xi_1 d\omega \\ &= \frac{3^{3/2}}{(2\pi)^{3/2}} \left(\frac{\sigma_2}{\sigma_1} \right)^3 f(\xi_1) P_1(\nu, \xi_1, \omega) \Theta(\omega) d\nu d\xi_1 d\omega, \end{aligned} \quad (57)$$

where $\Theta(\lambda_3) \Theta(\omega)$ is multiplied to pick peaks out of extrema, and the function f is given by

$$\begin{aligned} f(\xi_1) &:= \frac{5^{5/2}}{3\sqrt{2\pi}} \left(\int_0^{\xi_1/4} d\xi_2 \int_{-\xi_2}^{\xi_2} d\xi_3 + \int_{\xi_1/4}^{\xi_1/2} d\xi_2 \int_{3\xi_2 - \xi_1}^{\xi_2} d\xi_3 \right) \\ &\quad \left\{ \xi_2 (\xi_2^2 - \xi_3^2) \{(\xi_1 + \xi_3)^2 - 9\xi_2^2\} (\xi_1 - 2\xi_3) \exp \left[-\frac{15}{2}\xi_2^2 \right] \exp \left[-\frac{5}{2}\xi_3^2 \right] \right\} \\ &= \frac{1}{2} \xi_1 (\xi_1^2 - 3) \left(\text{erf} \left[\frac{1}{2} \sqrt{\frac{5}{2}} \xi_1 \right] + \text{erf} \left[\sqrt{\frac{5}{2}} \xi_1 \right] \right) \\ &\quad + \sqrt{\frac{2}{5\pi}} \left\{ \left(\frac{8}{5} + \frac{31}{4} \xi_1^2 \right) \exp \left[-\frac{5}{8}\xi_1^2 \right] + \left(-\frac{8}{5} + \frac{1}{2} \xi_1^2 \right) \exp \left[-\frac{5}{2}\xi_1^2 \right] \right\}. \end{aligned} \quad (58)$$

We note that, due to the condition $\lambda_3 > 0$ and $\omega > 0$, we obtain $\zeta_2 = \xi_1 \sigma_2 > 0$ and $\zeta_4 = -\omega \sigma_4 < 0$. Let us change the variables from $\xi_1 = \zeta_2 / \sigma_2$ and $\omega = -\zeta_4 / \sigma_4$ to variables μ and k_* defined in Eqs. (10) and (11)⁵. Using the variables ζ_0 , μ and k_* as the probability variables instead of ν , ξ_1 and ω , we obtain the following expression:

$$\begin{aligned} n_{\text{pk}}^{(k_*)}(\zeta_0, \mu, k_*) d\zeta_0 d\mu dk_* &:= n_{\text{pk}}(\nu, \xi_1, \omega) d\nu d\xi_1 d\omega \\ &= \frac{2 \cdot 3^{3/2}}{(2\pi)^{3/2}} \mu k_*^5 \frac{\sigma_2^2}{\sigma_0 \sigma_1^3 \sigma_4} f \left(\frac{\mu k_*^2}{\sigma_2} \right) P_1 \left(-\frac{\zeta_0}{\sigma_0}, \frac{\mu k_*^2}{\sigma_2}, \frac{\mu k_*^4}{\sigma_4} \right) d\zeta_0 d\mu dk_*. \end{aligned} \quad (59)$$

⁵ The linear relation $\delta \sim \Delta \zeta$ suggests that k_* is similar to the inverse length-scale of the density inhomogeneity $k_\delta \equiv (-\Delta \delta / \delta|_{\mathbf{x}=0})^{1/2}$. Using the non-linear relation between ζ and δ , we have

$$k_\delta^2 = \left(1 - \mu \left[2 - \frac{\zeta_2^{ij} \zeta_2^{ij}}{\zeta_2^2} \right] \right) k_*^2,$$

where summation of repeated indices is understood. Noting that $\zeta_2^2 \geq \zeta_2^{ij} \zeta_2^{ij}$, it is clear that k_* and k_δ will be similar for $\mu \ll 1$. However, the case of interest to us is $\mu > \mu_{\text{th}} \sim 0.5$. These are high peaks of the random distribution, and consequently they are nearly spherical. In this case, we can estimate $k_\delta^2 \approx (1 - 5\mu/3)k_*^2$, which becomes negative for $\mu > 3/5$. Since μ_{th} is smaller than $3/5$ in our setting, we do not have to worry about this peculiar regime, where the density profile has a local minimum at the center of the overdensity.

So far, the moments σ_n have been treated as constants which are independent of the probability variables such as ζ_0 , μ or k_* . However, in general, the moments depend on the comoving scale of the inhomogeneity given by $1/k_*$ through the smoothing scale introduced by a window function in the k -space integration. Let us redefine the moments as follows:

$$\sigma_n^2(k_*) = \int \frac{dk}{k} k^{2n} \mathcal{P}(k) W(k/k_*)^2, \quad (60)$$

where $W(k/k_*)$ is the window function. Therefore, hereafter, we treat the moments σ_n as functions of k_* . If we consider the $\mathcal{P}(k)W(k/k_*)^2$ as the effective power spectrum, introducing the window function is equivalent to considering a different power spectrum for each small k_* bin in Eq. (59).

Since the direct observable is not k_* but the PBH mass M , we further change the variable from k_* to M . Since the PBH mass is given by $M = \alpha/(2H)$ with α being a numerical factor, from the horizon entry condition (27), the PBH mass M can be expressed as follows:

$$\begin{aligned} M &= \frac{1}{2}\alpha H^{-1} = \frac{1}{2}\alpha \frac{\bar{a}\ell}{k_*} e^{-\mu g(\ell)} = \frac{1}{2}\alpha \frac{a\ell}{k_*} e^{-\zeta_0 - \mu g(\ell)} \\ &= \frac{1}{2}\alpha \frac{a k_* \ell}{k_*^2} e^{-\zeta_0 - \mu g(\ell)} = \frac{1}{2}\alpha \frac{a_{\text{eq}} k_{\text{eq}} \ell^2}{k_*^2} e^{-2(\zeta_0 + \mu g(\ell))} = M_{\text{eq}} \frac{k_{\text{eq}}^2}{k_*^2} \ell^2 e^{-2(\zeta_0 + \mu g(\ell))}, \end{aligned} \quad (61)$$

where we have used the fact $H \propto a^{-2}$ and $ak_* = a_{\text{eq}}^2 H_{\text{eq}} \ell e^{-\zeta_0 - \mu g(\ell)}$ with a_{eq} and H_{eq} being the scale factor and Hubble expansion rate at the matter-radiation equality. M_{eq} and k_{eq} are defined by $M_{\text{eq}} = \alpha H_{\text{eq}}^{-1}/2$ and $k_{\text{eq}} = a_{\text{eq}} H_{\text{eq}}$, respectively. The value of the numerical factor α is rather ambiguous, and we refer to the value $\alpha \sim 0.4$ presented in Ref. [32]. Solving the above equation for k_* , we obtain

$$k_* = k_{\text{eq}} \left(\frac{M_{\text{eq}}}{M} \right)^{1/2} \ell e^{-\zeta_0 - \mu g(\ell)}. \quad (62)$$

We change the variable k_* to M as follows:

$$\begin{aligned} n_{\text{pk}}^{(M)}(\zeta_0, \mu, M) d\zeta_0 d\mu dM &:= n_{\text{pk}}^{(k_*)}(\zeta_0, \mu, k_*) d\zeta_0 d\mu dk_* \\ &= \frac{3^{3/2} k_{\text{eq}}^6 M_{\text{eq}}^3 \ell^6}{(2\pi)^{3/2}} M^{-4} \mu e^{-6(\zeta_0 + \mu g(\ell))} \frac{\sigma_2^2}{\sigma_0 \sigma_1^3 \sigma_4} f\left(\frac{\mu k_*^2}{\sigma_2}\right) P_1\left(-\frac{\zeta_0}{\sigma_0}, \frac{\mu k_*^2}{\sigma_2}, \frac{\mu k_*^4}{\sigma_4}\right) d\zeta_0 d\mu dM, \end{aligned} \quad (63)$$

where the moments σ_n and k_* should be regarded as functions of ζ_0 , μ and M . The number density of PBHs is given by

$$n_{\text{BH}} d \ln M = \left[\int_{-\infty}^{\infty} d\zeta_0 \int_{\mu_{\text{th}}}^{\infty} d\mu n_{\text{pk}}^{(M)}(\zeta_0, \mu, M) \right] M d \ln M. \quad (64)$$

We also note that the scale factor a is a function of M as $a = 2M^{1/2}M_{\text{eq}}^{1/2}k_{\text{eq}}/\alpha$. Then, the fraction of PBHs to the total density $\beta_0 d \ln M$ can be given by

$$\beta_0 d \ln M = \frac{M n_{\text{BH}}}{\rho a^3} d \ln M = \frac{4\pi}{3} \alpha q^{-3} n_{\text{BH}} k_{\text{eq}}^{-3} \left(\frac{M}{M_{\text{eq}}} \right)^{3/2} d \ln M$$

$$\begin{aligned}
&= \frac{2 \cdot 3^{1/2} \alpha k_{\text{eq}}^3 \ell^6}{(2\pi)^{1/2}} \left(\frac{M_{\text{eq}}}{M} \right)^{3/2} \left[\int_{-\infty}^{\infty} d\zeta_0 \int_{\mu_{\text{th}}}^{\infty} d\mu \mu e^{-6(\zeta_0 + \mu g(\ell))} \right. \\
&\quad \left. \frac{\sigma_2^2}{\sigma_0 \sigma_1^3 \sigma_4} f\left(\frac{\mu k_*^2}{\sigma_2}\right) P_1\left(-\frac{\zeta_0}{\sigma_0}, \frac{\mu k_*^2}{\sigma_2}, \frac{\mu k_*^4}{\sigma_4}\right) \right] d\ln M. \quad (65)
\end{aligned}$$

Here, we summarize how to use the above formula. In order to calculate the PBH fraction, the necessary ingredients are the threshold of the density perturbation δ_{th} , a plausible functional form of $g(k_*r)$, the curvature power spectrum $\mathcal{P}(k)$ and the window function $W(k/k_*)$. The moments σ_n can be calculated from Eq. (60) as a function of k_* . Then, k_* should be expressed as a function of ζ_0 , μ and M by Eq. (62). The probability distribution function P_1 is defined in Eq. (49). The value of ℓ is given by the root of Eq. (23). The value of μ_{th} is calculated from δ_{th} through Eq. (26). Substituting all expressions listed above into Eq. (65), we can evaluate the PBH fraction.

In the numerical examples that follow, we will assume $\alpha = 0.4$. For the density threshold we will take $\delta_{\text{th}} \approx 0.533$. Some examples for the function $g(k_*r)$ are listed in Appendix C. A plausible functional form is the following:

$$g(k_*r) = 1 - \text{sinc}(k_*r), \quad (66)$$

which, as mentioned at the end of Section II B, corresponds to the monochromatic power spectrum. In this case, we obtain

$$\ell \simeq 2.74 \quad (67)$$

$$\mu_{\text{th}} \simeq 0.941 - 0.665\sqrt{2 - 3\delta_{\text{th}}}. \quad (68)$$

For $\delta_{\text{th}} \approx 0.533$, we obtain $\mu_{\text{th}} \approx 0.520$.

B. Estimation from the Press-Schechter formalism

For a comparison, we review a conventional estimate of the fraction of PBHs based on the PS formalism. Let us start from the following Gaussian distribution assumption for the density perturbation δ .

$$P_{\delta}(\delta) d\delta = \frac{1}{\sqrt{2\pi}\sigma_{\delta}} \exp\left(-\frac{1}{2}\frac{\delta^2}{\sigma_{\delta}^2}\right) d\delta, \quad (69)$$

where σ_{δ} is given by the coarse-grained density contrast

$$\sigma_{\delta}(k_*) = \frac{4}{9} \frac{\sigma_2(k_*)}{k_*^2} \quad (70)$$

with a smoothing inverse lengthscale k_* . This Gaussian distribution and the dispersion are motivated by the linear relation between ζ and δ . The fraction β_0^{PS} is then evaluated as follows:

$$\beta_{0,\delta}^{\text{PS}}(M) = 2\alpha \int_{\delta_{\text{th}}}^{\infty} d\delta P_{\delta}(\delta) = \alpha \text{erfc}\left(\frac{\delta_{\text{th}}}{\sqrt{2}\sigma_{\delta}(k_M)}\right) = \alpha \text{erfc}\left(\frac{9}{4}\frac{\delta_{\text{th}} k_M^2}{\sqrt{2}\sigma_2(k_M)}\right). \quad (71)$$

with the smoothing inverse lengthscale k_M given by

$$k_M = k_{\text{eq}}(M_{\text{eq}}/M)^{1/2}. \quad (72)$$

Note, in particular, that the smoothing scale k_M differs from k_* given in (62) by the factor $\ell e^{-\zeta_0 - \mu g(\ell)}$. The fraction f_0^{PS} at the equality time is given by $f_{0,\delta}^{\text{PS}} = (M_{\text{eq}}/M)^{1/2} \beta_0^{\text{PS}}$.

Let us consider another way of estimation as a reference. Since we have introduced the threshold value μ_{th} in Sec. IV B, let us consider the following Gaussian distribution of μ

$$P_\mu(\mu) d\mu = \frac{1}{\sqrt{2\pi}\sigma_2} \exp\left(-\frac{1}{2}\frac{\mu^2 k_M^4}{\sigma_2^2}\right) d\mu. \quad (73)$$

As in the case of $\beta_{0,\delta}^{\text{PS}}$, we can evaluate the PBH fraction $\beta_{0,\mu}^{\text{PS}}$ as follows:

$$\beta_{0,\mu}^{\text{PS}}(M) = 2\alpha \int_{\mu_{\text{th}}}^{\infty} d\mu P_\mu(\mu) = \alpha \text{erfc}\left(\frac{\mu_{\text{th}} k_M^2}{\sqrt{2} \sigma_2(M)}\right). \quad (74)$$

We note that, in our setting, $\mu_{\text{th}} \approx 0.520 < 9\delta_{\text{th}}/4 \approx 1.20$. This simple analysis clearly indicates that the optimized criterion given in Sec. II B will significantly increase the PBH fraction compared to the conventional estimate (71). This will now be shown from a numerical study.

C. Monochromatic power spectrum

Let us consider the monochromatic power spectrum given by

$$\mathcal{P}(k) = \sigma_0^2 k_0 \delta(k - k_0). \quad (75)$$

Then, the moments are calculated as

$$\sigma_n^2 = \sigma_0^2 k_0^{2n}. \quad (76)$$

The value of γ_n is given by 1. Taking the limit $\gamma_n = \gamma \rightarrow 1$, in the expression (49), we obtain

$$\begin{aligned} & \lim_{\gamma_n \rightarrow 1} P_1(\nu, \xi_1, \omega) \\ &= \lim_{\gamma \rightarrow 1} \frac{(2\pi)^{-3/2}}{\sqrt{3}(1-\gamma)} \exp\left[-\frac{1}{2} \left\{ \frac{2}{3} \frac{1}{1-\gamma} \left(\nu - \frac{1}{2}\xi_1 - \frac{1}{2}\omega \right)^2 + \frac{1}{2} \frac{1}{1-\gamma} (\xi_1 - \omega)^2 + \omega^2 \right\} \right] \\ &= \frac{(2\pi)^{-1/2}}{2\mu} k_0 \sigma_0^2 \delta(\zeta_0 + \mu) \delta(k_* - k_0) \exp\left(-\frac{\mu^2}{2\sigma_0^2}\right). \end{aligned} \quad (77)$$

Then, we obtain

$$\begin{aligned} \beta_0 d \ln M &= \frac{3^{1/2} \alpha \ell^6}{2\pi \sigma_0} \left(\frac{M_{\text{eq}}}{M} \right)^{3/2} \left(\frac{k_{\text{eq}}}{k_0} \right)^3 k_0 \\ &\times \int_{\mu_{\text{th}}}^{\infty} e^{6\mu(1-g(\ell))} f\left(\frac{\mu}{\sigma_0}\right) \delta(k_* - k_0) \exp\left[-\frac{\mu^2}{2\sigma_0^2}\right] d\mu d \ln M. \end{aligned} \quad (78)$$

Since the condition $k_* = k_0$ can be rewritten as

$$\mu = \mu_0 := \frac{1}{2(1-g(\ell))} \ln \left(\frac{M}{M_{\text{eq}}} \frac{k_0^2}{k_{\text{eq}}^2} \frac{1}{\ell^2} \right), \quad (79)$$

we find the following relation

$$\delta(k_* - k_0) = \frac{1}{k_0(1-g(\ell))} \delta(\mu - \mu_0). \quad (80)$$

Then, β_0 can be calculated as

$$\begin{aligned} \beta_0 d \ln M &= \frac{3^{1/2} \alpha}{2\pi \sigma_0} \frac{1}{1-g(\ell)} \left(\frac{M}{M_{\text{eq}}} \right)^{3/2} \left(\frac{k_0}{k_{\text{eq}}} \right)^3 \\ &\quad \times f \left(\frac{\mu_0}{\sigma_0} \right) \exp \left(-\frac{\mu_0^2}{2\sigma_0^2} \right) \Theta(M - M_{\text{th}}) d \ln M, \end{aligned} \quad (81)$$

where

$$M_{\text{th}} = M_{\text{eq}} \left(\frac{k_{\text{eq}}}{k_0} \right)^2 \ell^2 e^{2\mu_{\text{th}}(1-g(\ell))}. \quad (82)$$

At $M = M_{\text{th}}$, the value of β_0 is given by

$$\beta_0|_{M=M_{\text{th}}+0} = \frac{\sqrt{3}\alpha}{2\pi q^3 \sigma_0} \frac{\ell^3}{1-g(\ell)} e^{3\mu_{\text{th}}(1-g(\ell))} f \left(\frac{\mu_{\text{th}}}{\sigma_0} \right) \exp \left(-\frac{\mu_{\text{th}}^2}{2\sigma_0^2} \right). \quad (83)$$

Since the function $f(x)$ behaves like $f(x) \sim x^3$ for $x \gg 1$ [42], in the limit of small σ_0 , we obtain

$$\beta_0 \sim \frac{\mu_{\text{th}}^3}{\sigma_0^4} e^{3\mu_{\text{th}}(1-g(\ell))} \exp \left(-\frac{\mu_{\text{th}}^2}{2\sigma_0^2} \right). \quad (84)$$

The mass spectra β_0 and f_0 are depicted as functions of the PBH mass M for $\sigma_0 = 0.08$, 0.06 and 0.05 in the left panels of Figs. 1 and 2, while β_0 and f_0 are depicted as functions of σ_0 for $M = M_{\text{th}}$ in the right panels of Figs. 1 and 2. As a result, we obtain an extended mass spectrum of PBHs even for the monochromatic power spectrum of the curvature perturbation. This is caused by the non-linear relation between the density perturbation and the curvature perturbation through Eq. (61).

Note that the amplitude of the mass spectrum is huge compared to the conventional one $\beta_{0,\delta}^{\text{PS}}$ for a small value of σ_0 . The main reason for this deviation comes from the optimization of the PBH formation threshold μ_{th} . The σ_0^{-4} dependence of the prefactor in Eq. (84) also contributes to increase the fraction, but not so dramatically. We note that the strong enhancement in the abundance of PBH is a robust feature, for any chosen value of the threshold δ_{th} . Indeed, it follows from (68) that for $\delta_{\text{th}} < \delta_{\text{max}} = 2/3$, we have $\mu_{\text{th}} < (9/4)\delta_{\text{th}}$. According to Eqs. (71) and (74), this implies $\beta_{0,\mu}^{\text{PS}}(M) \gg \beta_{0,\delta}^{\text{PS}}(M)$. In fact, for $\delta_{\text{th}} < 0.623$, we have $\mu_{\text{th}} < (9/8)\delta_{\text{th}}$ (the right hand side of this inequality is actually a good linear fit to the value of μ_{th} , which typically overestimates the actual value by less than 30%). Assuming that the probability of PBH formation is low, We can approximate the complementary error function as $\text{erfc}(x) \approx e^{-x^2}/(\sqrt{\pi}x)$, and it follows that within this range of δ_{th} we have

$$\beta_{0,\mu}^{\text{PS}}(M) \gg (\beta_{0,\delta}^{\text{PS}}(M))^{1/4}, \quad (85)$$

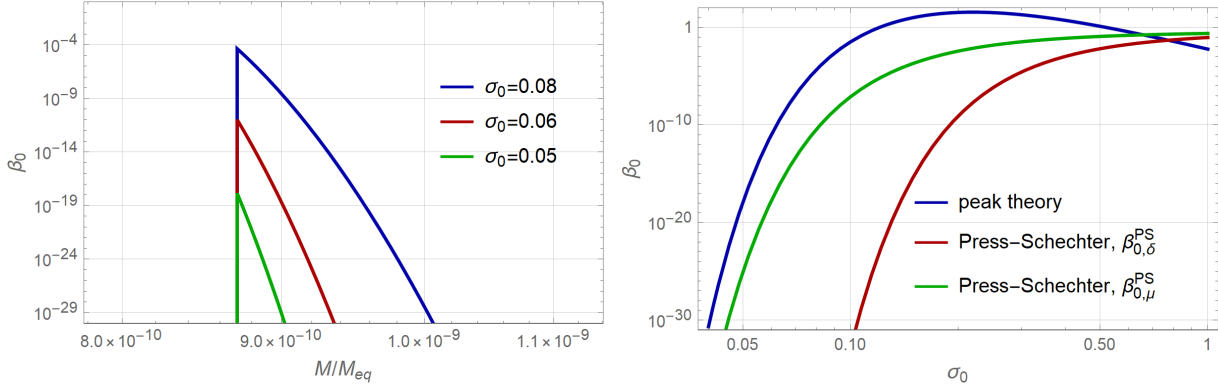


FIG. 1. PBH fraction to the total density β_0 at the formation time is depicted as a function of the PBH mass M (left panel) for each value of σ_0 , and a function of σ_0 (right panel) for $M = M_{\text{th}}$ with $k_0 = 10^5 k_{\text{eq}}$ and $\alpha = 0.4$. We also depict the conventional estimation from the PS formalism in the right panel.

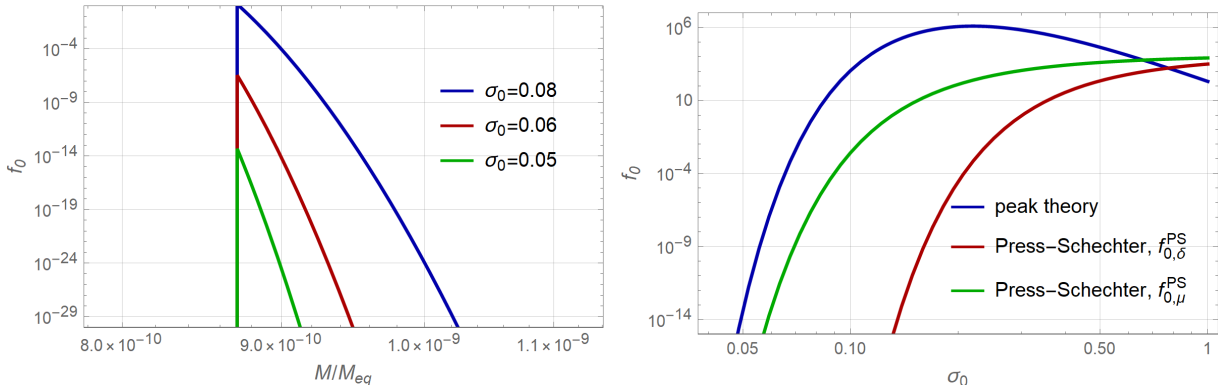


FIG. 2. PBH Fraction to the total density f_0 at the equality time is depicted as a function of the PBH mass M (left panel) for each value of σ_0 , and a function of σ_0 (right panel) for $M = M_{\text{th}}$ with $k_0 = 10^5 k_{\text{eq}}$ and $\alpha = 0.4$. We also depict the conventional estimation from the PS formalism in the right panel.

where we have ignored the sub-exponential dependence. Given that the probability of PBH formation is exponentially small, this represents a very strong enhancement.

Furthermore, there is a non-trivial correction to the expression for the mass in terms of the wave number at the time of horizon crossing, which enhances the mass of the black holes by one order of magnitude or so relative to the expectation from linear theory. This is clear from the expression of M_{th} given in Eq. (82), which contains the factor $\ell^2 e^{2\mu_{\text{th}}(1-g(\ell))} \approx 8.7$. Here, we have used the numerical values for μ_{th} , ℓ and $g(\ell)$ corresponding to the sinc profile, which is the appropriate one for the monochromatic spectrum. These values are listed in Table I of Appendix C. Hence, not only do we find more PBHs, but they are also significantly larger than naively expected.

D. An extended power spectrum

Let us consider the simple extended power spectrum given by

$$\mathcal{P}(k) = \sigma^2 \left(\frac{k}{k_0} \right)^2 \exp \left(-\frac{k^2}{k_0^2} \right), \quad (86)$$

and the Gaussian window function $W_G(k/k_*)$ defined as

$$W_G(k/k_*) = \exp \left(-\frac{1}{2} \frac{k^2}{k_*^2} \right). \quad (87)$$

Then, each moment can be calculated as follows:

$$\sigma_n^2 = \int \frac{dk}{k} k^{2n} \mathcal{P}(k) W_G^2 = \frac{n\Gamma(n)\sigma^2}{2k_0^2} \left(\frac{1}{k_0^2} + \frac{1}{k_*^2} \right)^{-n-1}, \quad (88)$$

where Γ means the gamma function. The mass spectra β_0 and f_0 are depicted in Fig. 3 for $\sigma = 0.15, 0.2$ and 0.3 with $k_0 = 10^5 k_{\text{eq}}$ and $\alpha = 0.4$. We note that the conventional mass spectrum $\beta_{0,\delta}^{\text{PS}}$ evaluated by using the Gaussian distribution of δ is much smaller and deviates from the plot region. Therefore, we plot only $\beta_{0,\mu}^{\text{PS}}$ for a reference. The mass spectrum f_0 shown in Fig. 3 can be directly constrained by observations. Here, we note that σ_δ defined in Eq. (70) should be regarded as a function of the smoothing inverse lengthscale k_* with the redefinition of the moments (88). The maximum value of σ_δ as a function of k_* is given by $8\sigma/(27\sqrt{3})$ at $k_* = k_0/\sqrt{2}$. For $\sigma = 0.3$, the maximum value is given by 0.0513.

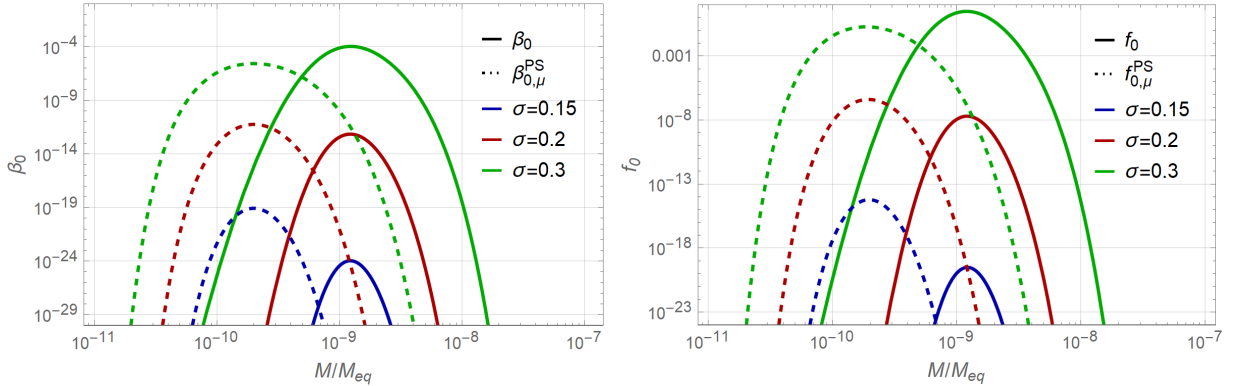


FIG. 3. The fraction of PBHs to the total density at the formation time (β_0 , $\beta_{0,\mu}^{\text{PS}}$) and at the matter-radiation equality time (f_0 , $f_{0,\mu}^{\text{PS}}$) are depicted as functions of the PBH mass M for $\sigma = 0.4$, $k_0 = 10^5 k_{\text{eq}}$, $q = 1$ and $\alpha = 0.4$.

Although we can calculate f_0 , which can be directly constrained by observations, it is not easy to understand the behavior of the mass spectrum f_0 from the direct comparison between $f_{0,\mu}^{\text{PS}}$ and f_0 . In order to understand the results, it is helpful to consider the conditional

probability with fixed k_* . First, we re-express the probability P_1 as a probability distribution function \tilde{P}_1 of ζ_0 , μ and k_* , that is

$$\tilde{P}_1(\zeta_0, \mu, k_*) d\zeta_0 d\mu dk_* = P_1(\nu, \xi_1, \omega) d\nu d\xi_1 d\omega = \frac{2|\mu|k_*^5}{\sigma_0\sigma_2\sigma_4} P_1\left(-\frac{\zeta_0}{\sigma_0}, \frac{\mu k_*^2}{\sigma_2}, \frac{\mu k_*^4}{\sigma_4}\right) d\zeta_0 d\mu dk_*. \quad (89)$$

Then, the conditional probability $p_1(\zeta_0, \mu)$ with fixed k_* is given by

$$p_1(\zeta_0, \mu) \propto |\mu| \exp\left[-\frac{1}{2} \left\{ \frac{1 - \gamma_3^2}{D\sigma_0^2} (\zeta_0 - \bar{\zeta}_0)^2 + \frac{\mu^2}{\tilde{\sigma}^2} \right\}\right], \quad (90)$$

where

$$\bar{\zeta}_0 = -\frac{(\sigma_1^2\sigma_4^2 - \sigma_2^2\sigma_3^2)k_*^2 + (\sigma_2^4 - \sigma_1^2\sigma_3^2)k_*^4}{\sigma_2^2\sigma_4^2 - \sigma_3^4}\mu, \quad (91)$$

$$\frac{1}{\tilde{\sigma}^2} = k_*^4 \left(\frac{\sigma_4^2 - 2\sigma_3^2k_*^2 + \sigma_2^2k_*^4}{\sigma_2^2\sigma_4^2 - \sigma_3^4} \right). \quad (92)$$

Integrating $p_1(\zeta_0, \mu)$ with respect to ζ_0 and normalizing it, we obtain the following conditional probability distribution function $p(\mu)$:

$$p(\mu) d\mu = \frac{1}{2} \left| \frac{\mu}{\tilde{\sigma}} \right| \exp\left(-\frac{1}{2} \frac{\mu^2}{\tilde{\sigma}^2}\right) d\left(\frac{\mu}{\tilde{\sigma}}\right). \quad (93)$$

The integration in the region above the threshold μ_{th} can be calculated as

$$\beta_0^{\text{CP}}(M) = \frac{1}{2} \exp\left(-\frac{1}{2} \frac{\mu_{\text{th}}^2}{\tilde{\sigma}^2|_{k_* \rightarrow k_M}}\right), \quad (94)$$

where we have described β_0^{CP} as a function of M by replacing $k_* \rightarrow k_M$, given by Eq. (72) rather than Eq. (62). The reason is that we want to compare the conditional probability distribution with the PS distribution, by using the same smoothing scale in both cases. In the left panel of Fig. 4, $\beta_{0,\mu}^{\text{PS}}$ and β_0^{CP} are depicted as functions of M for $\sigma = 0.15, 0.2$ and $\sigma = 0.3$. Comparing $\beta_{0,\mu}^{\text{PS}}$ and β_0^{CP} , we find the deviations of the spectrum peaks. This deviation reflects the difference between the shapes of $\tilde{\sigma}$ and σ_2/k_*^2 as functions of k_* shown in the right panel of Fig. 4.

Next, let us compare β_0 and β_0^{CP} . In Fig. 5, β_0 and β_0^{CP} are depicted as functions of M for $\sigma = 0.15, 0.2$ and $\sigma = 0.3$. There are two main differences between β_0 and β_0^{CP} . First of all, the spectrum is shifted to the larger mass by about one order of magnitude. The origin of this effect is the factor $\ell^2 e^{-2(\zeta_0 + \mu g(\ell))}$ in the relation (61) between k_* and M . The second difference is the enhancement of the abundance at the peak of the mass spectrum. This enhancement mainly comes from the factor $f(\mu k_*^2/\sigma_2)$. Since the function $f(x)$ behaves like $f(x) \sim x^3$ for $x \gg 1$, the factor $f(\mu k_*^2/\sigma_2) \sim 10^3$ in the parameters chosen in Fig. 4. This factor appears through integration with respect to ξ_2 and ξ_3 in Eq. (58). In the integration (58), the only nontrivial contribution comes from the factor (56) in the integrand. This ξ dependent factor describes the difference of the measure in the real space and the parameter space of η . The integral range of ξ_2 and ξ_3 in Eq. (58) becomes larger for larger $\xi_1 = k_*^2\mu/\sigma_2$.

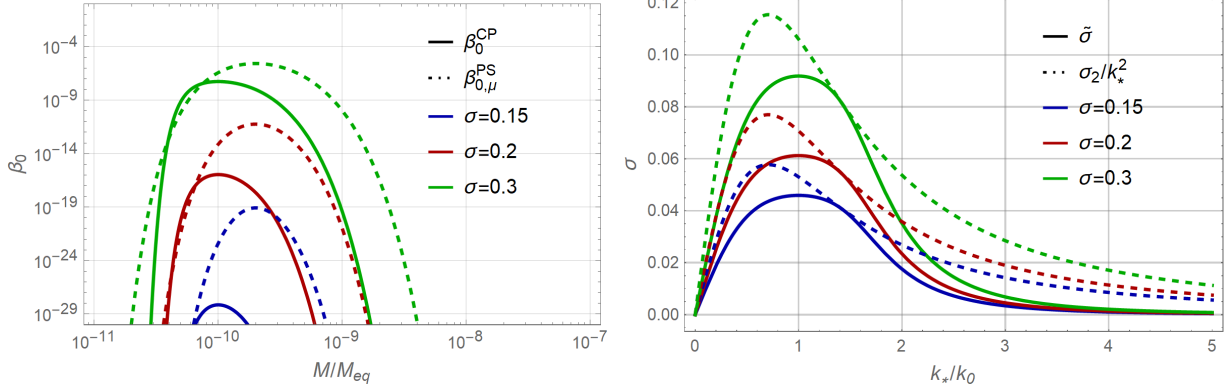


FIG. 4. β_0^{CP} (solid lines) and $\beta_{0,\mu}^{\text{PS}}$ (dashed lines) as functions of M for $\sigma = 0.3, 0.4$ and 0.5 (left panel), and $\tilde{\sigma}$, and σ_2/k_*^2 as functions of k_* (right panel).

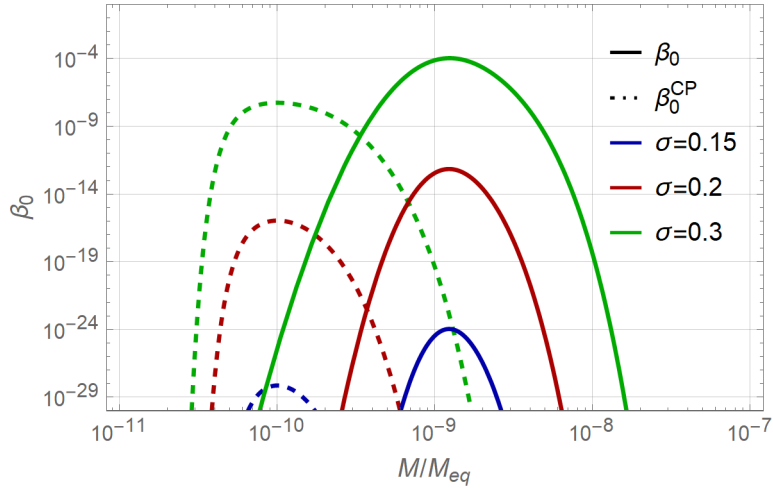


FIG. 5. β_0 (solid lines) and β_0^{CP} (dashed lines) as functions of M for $\sigma = 0.15, 0.2$ and 0.3 , respectively.

Since the values of ξ_2 and ξ_3 describe the non-sphericity of the configuration, the range of ξ_2 and ξ_3 shows how large non-spherical deformation is possible with keeping the value of ξ_1 . In summary, the enhancement comes from the higher deformability of the peak for a large enough density perturbation to form a PBH in association with the measure difference between the real space and the parameter space of η .

Finally, let us discuss the window function dependence of the mass spectrum. It is well known that in the PS formalism the mass spectrum significantly depends on the choice of the window function [45]. A similar dependence occurs in our case. Following Ref. [45], let

us consider two window functions different from the Gaussian in (87):

$$W_{\text{RTH}}(k/k_*) = 3 \frac{\sin(k/k_*) - k/k_* \cos(k/k_*)}{k^3/k_*^3}, \quad (95)$$

$$W_{k\text{TH}}(k/k_*) = \Theta(k_* - k), \quad (96)$$

where W_{RTH} and $W_{k\text{TH}}$ are the real-space top-hat(RTH) and the k -space top-hat(k TH) window functions, respectively. The corresponding moments $\sigma_n(k_*)$ can be numerically calculated like in Eq. (88), and we can obtain the value of $\tilde{\sigma}$ defined in Eq. (92) as a function of k_* . In Fig. 6, the values of $\tilde{\sigma}$ (left panel), and σ_2/k_*^2 (right panel) are depicted as functions of k_* for the three different window functions. As is in the case of σ_2/k_*^2 used in the PS

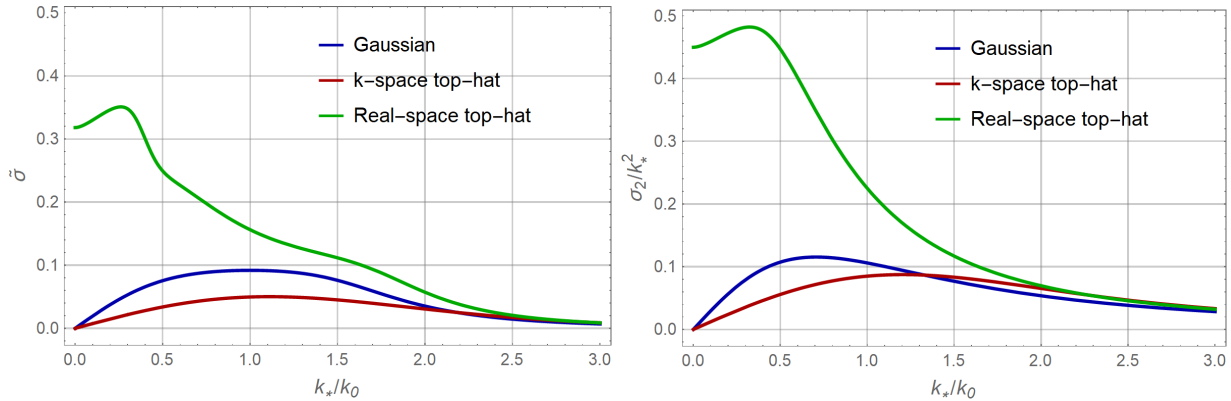


FIG. 6. $\tilde{\sigma}$ and σ_2/k_*^2 as functions of k_* for three different window functions.

formalism, we see that the values of $\tilde{\sigma}$ may be different by a sizable factor. Obviously, this factor causes a significant order of magnitude difference in the fraction of PBHs β_0 and f_0 through the exponential dependence found in Eq. (93).

It should be noted, however, that the unusual behaviour of the RTW window function may be attributed to a significant tail at large momenta $k \gg k_*$, where it decreases only as a power law. Note, in particular, that the integrand in Eq. (88) for $n=2$ is completely unsuppressed for $k_* \ll k \ll k_0$. The contribution of high momenta is due to the sharp edges of the RTH window function in real space. In this sense, the Gaussian or the k TH window functions seem to do a better job of selecting the relevant contributions from the power spectrum.

V. SUMMARY AND DISCUSSION

Primordial black holes (PBHs) have attracted much attention not only from a theoretical point of view but also observationally. In order to make an observationally relevant prediction from a theoretical result, the estimation of the abundance of PBHs is essential.

The conventional Press-Schechter(PS) formalism assumes a Gaussian distribution of the primordial density or curvature perturbation. However, the threshold value of the curvature

perturbation has an ambiguity from environmental effects [39, 40]. On the other hand, the existence of an upper limit for the density perturbation at the time of horizon entry [41] is in conflict with the naive assumption of a Gaussian probability distribution for such variable.

In order to overcome the above issues, we have developed a formalism to estimate the abundance of PBHs by combining the Gaussian probability distribution of the curvature perturbation with a threshold value for the locally averaged density perturbation. More precisely, we consider an optimized criterion for PBH formation which uses the maximum compaction radius proposed in Ref. [30]. Our approach is based on the peak theory of Gaussian random fields [42], and takes into consideration the non-linear relation between the curvature perturbation and the density perturbation. A general expression for the fraction of PBHs to the total density of the Universe is presented, in terms of the gradient moments of the curvature power spectrum up to the 4-th order.

The case of the monochromatic power spectrum is particularly simple, and illustrative of the general case. First of all, compared to the conventional PS approach, the PBH spectrum is shifted to larger masses, by an order of magnitude or so. This is due to the non-trivial correction to the relation between the co-moving wavelength and the mass at the time of horizon crossing, which is substantially affected by the metric perturbation. A related effect is that there is a slight spread in the mass spectrum, even when the underlying primordial spectrum is monochromatic. Such spread, however is hardly significant. Finally, the estimated abundance of PBH is much larger than in the conventional PS formalism, by many orders of magnitude. This effect comes mainly from the optimized PBH formation criterion. Roughly speaking, in the limit when the probability of PBH formation is exponentially low, our estimate for such probability is larger than the fourth root of the conventional result. Therefore, the effect is very significant. We have also considered the case of an extended power spectrum, which displays qualitatively similar effects.

Throughout this paper we have assumed that the criterion for the formation of PBHs can be given in terms of a threshold for the amplitude of some (averaged) density perturbation. However, it is known that such threshold depends on the profile of the overdensity. In order to clarify such dependence, we need an analysis including higher orders of the Taylor expansion given in Eq. (3), combined with numerical simulations. There is also a significant dependence of the PBH abundance on the window function which is used for computing the moments from the curvature power spectrum, as recently emphasized in Ref. [45] in the PS context. It should be stressed, nonetheless, that the strong enhancement of the abundance of PBH and the shift of the spectrum to higher masses are present already in the monochromatic case, where there is no ambiguity in the profile of the high peaks, and where there is no need for a window function.

Another interesting aspect to consider is the effect of a non-Gaussianity the primordial curvature probability distribution, which may cause enhancement/suppression of the abundance of PBHs and clustering of PBHs. Such issues are left for further research.

ACKNOWLEDGEMENTS

We thank T. Hiramatsu, I. Musco, M. Sasaki, T. Takeuchi and T. Tanaka for helpful comments. This work was supported by JSPS KAKENHI Grant Numbers JP16K17688, JP16H01097 (C.Y.), JP26400282 (T.H.), JP17H01131 (K.K.), 26247042 (K.K.), and MEXT KAKENHI Grant Numbers JP15H05889(K.K.), and JP16H0877 (K.K.) FPA2016-76005-C2-2-P, MDM-2014-0369 of ICCUB (Unidad de Excelencia Maria de Maeztu), AGAUR 2014-SGR-1474 (J.G.). The authors thank the Yukawa Institute for Theoretical Physics at Kyoto University. Discussions during YITP-T-17-02 “Gravity and Cosmology 2018” and the YITP symposium YKIS2018a “General Relativity – The Next Generation –” were useful to complete this work.

Appendix A: Deviation between peaks of ζ and δ

Our analysis is based on the Taylor expansion around a peak of ζ . However, since the criterion for a formation of PBHs is given in terms of δ , one may concern about the deviation between each peak of ζ and δ . Here, assuming the all moments σ_n are far smaller than $k_*^n \sim (\bar{a}H)^n$ at the horizon entry, we show that, if the value of δ is comparable to the threshold value δ_{th} at a peak, we can almost always find the associated peak of ζ well inside the horizon patch centered at the peak of δ . This fact means that the region which allows the formation of PBHs typically involves peaks of δ and ζ near the center, and validates our procedure.

Let us consider a peak of δ (not peak of ζ) satisfying $\delta > \delta_{\text{th}}$. The value of δ can be expressed in terms of the Taylor expansion around the peak as follows:

$$\delta = \frac{2(1+w)}{3w+5} \frac{1}{a^2 H^2} \left[e^{2\zeta_0} \left(\zeta_2 - \frac{1}{2} \sum_i \zeta_1^i \right) \right] + \mathcal{O}(y^2), \quad (\text{A1})$$

where we have introduced a new spatial coordinate \mathbf{y} to emphasize the difference from the expansion around the peak of ζ adopted in the text. From the inequality $\delta > \delta_{\text{th}}$, we obtain the following inequality:

$$\zeta_2 > \frac{3w+5}{2(1+w)} \bar{a}^2 H^2 \delta_{\text{th}} \gg \sigma_2, \quad (\text{A2})$$

where and hereafter we evaluate every variable at the horizon entry, that is, $k_* \sim \bar{a}H$. The deviation Δy_j of the peak of ζ from the peak of δ can be estimated by the following equation:

$$\sum_j \Delta y_j \zeta_2^{ji} = -\zeta_1^i. \quad (\text{A3})$$

Taking the principal direction of ζ_2^{ij} , we obtain

$$\zeta_2^{ij} = \text{diag} \{ \lambda_1, \lambda_2, \lambda_3 \}. \quad (\text{A4})$$

Since $\zeta_2 \gg \sigma_2$, from the probability distribution of $P_2(\xi_2, \xi_3, \boldsymbol{\eta})$, we can find that the probability to have a negative eigen value is typically very small. Then, we obtain the following equation:

$$|\Delta y_i| = |\zeta_1^i / \lambda_i| \lesssim \sigma_1 / k_*^2 \ll 1 / (\bar{a}H), \quad (\text{A5})$$

where we have used $\lambda_i \sim \zeta_2 \gtrsim k_*^2$ and $\zeta_1^i \sim \sqrt{<\zeta_1^i \zeta_1^i>} \sim \sigma_1$.

Appendix B: Correspondence with 3-zone model

Let us consider the corresponding parameters to ζ_0 , μ and k_* in 3-zone model[38]. In the 3-zone model, we consider the closed FLRW model as the collapsing region. The line element can be written as the following forms:

$$ds_3^2 = a^2 \left(\frac{d\bar{r}^2}{1 - \bar{r}^2} + \bar{r}^2 d\Omega^2 \right) \quad (\text{B1})$$

$$= a^2 e^{-2\zeta} (dr^2 + r^2 d\Omega^2). \quad (\text{B2})$$

From the metric forms, we obtain the following relations:

$$\frac{d\bar{r}}{\sqrt{1 - \bar{r}^2}} = \pm e^{-\zeta} dr, \quad (\text{B3})$$

$$\frac{\bar{r}}{r} = e^{-\zeta}. \quad (\text{B4})$$

Then, we obtain

$$\frac{r}{C} = \begin{cases} \frac{2\bar{r}}{1 + \sqrt{1 - \bar{r}^2}} & \text{for } r \leq 2C \\ \frac{2(1 + \sqrt{1 - \bar{r}^2})}{\bar{r}} & \text{for } 2C < r \end{cases}, \quad (\text{B5})$$

$$\bar{r} = \frac{4r/C}{4 + (r/C)^2} \quad (\text{B6})$$

and

$$e^{-\zeta} = \frac{\bar{r}}{r} = \frac{4/C}{4 + (r/C)^2}, \quad (\text{B7})$$

where C is the integration constant. This constant is related to ζ_0 as $e^{-2\zeta_0} = 1/C^2$ and can be absorbed into the renormalized scale factor \bar{a} as in the text or equivalently into the rescaling of the radial coordinate. Therefore, hereafter, we set $C = 1$ for simplicity.

The value of $\Delta\zeta$ at the origin can be evaluated as

$$\Delta\zeta|_{\bar{r}=0} = \frac{3}{2} = \mu k_*^2, \quad (\text{B8})$$

where we have identified it as μk_*^2 as in the text. From the Hubble equation, the density perturbation δ^{CMC} in the uniform Hubble slice is given by

$$\delta^{\text{CMC}} = \frac{8\pi\rho}{3H^2} - 1 = \frac{1}{a^2 H^2}. \quad (\text{B9})$$

If we adopt the definition of the horizon entry $1/k_* \sim \bar{r}$, we obtain

$$\frac{2}{3}\mu = \frac{1}{k_*^2} \sim \bar{r}_*^2 < 1. \quad (\text{B10})$$

That is, we do not have the horizon entry time for $\mu > \frac{3}{2}$ which corresponds to Type II PBH formation.

Appendix C: examples of the function $g(k_*r)$

Here we list some examples of the function $g(x)$.

- Sinc function

$$g(x) = 1 - \text{sinc}(x) = \sum_{n=1}^{\infty} \left[\frac{(-1)^{n-1}}{(2n+1)!} x^{2n} \right]. \quad (\text{C1})$$

- up to 4th order

$$g(x) = \sum_{n=1}^2 \left[\frac{(-1)^{n-1}}{(2n+1)!} x^{2n} \right] = \frac{1}{6}x^2 - \frac{1}{120}x^4. \quad (\text{C2})$$

- up to 8th order

$$g(x) = \sum_{n=1}^4 \left[\frac{(-1)^{n-1}}{(2n+1)!} x^{2n} \right]. \quad (\text{C3})$$

- Gaussian

$$g(x) = \frac{5}{3} (1 - \exp(-x^2/10)). \quad (\text{C4})$$

The values of ℓ , $g(\ell)$, μ_{th} and $\ell^2 e^{2\mu_{\text{th}}(1-g(\ell))}$ are listed in Table I. According to Eq. (82), the latter column represents the enhancement in the black hole mass relative to the naive linear estimate. Note that this effect is of a similar magnitude in all four examples.

TABLE I. The values of ℓ , $g(\ell)$, μ_{th} and $\ell^2 e^{2\mu_{\text{th}}(1-g(\ell))}$ for the listed examples with $\delta_{\text{th}} \approx 0.533$.

	ℓ	$g(\ell)$	μ_{th}	$\ell^2 e^{2\mu_{\text{th}}(1-g(\ell))}$
sinc	2.74	0.859	0.520	8.72
4th order	$\sqrt{5} \simeq 2.24$	$5/8 = 0.625$	0.663	8.22
8th order	2.72	0.849	0.522	8.66
Gaussian	$\sqrt{10} \simeq 3.16$	$5(1 - 1/e)/3 \simeq 1.05$	0.450	9.53

[1] Y. B. Zel'dovich and I. D. Novikov, Soviet Ast. **10**, 602 (1967), *The Hypothesis of Cores Retarded during Expansion and the Hot Cosmological Model*.

- [2] S. Hawking, Mon. Not. Roy. Astron. Soc. **152**, 75 (1971), *Gravitationally collapsed objects of very low mass*.
- [3] B. J. Carr, K. Kohri, Y. Sendouda, and J. Yokoyama, Phys. Rev. **D81**, 104019 (2010), arXiv:0912.5297, *New cosmological constraints on primordial black holes*.
- [4] B. Carr, F. Kuhnel, and M. Sandstad, Phys. Rev. **D94**, 083504 (2016), arXiv:1607.06077, *Primordial Black Holes as Dark Matter*.
- [5] G. F. Chapline, Nature **253** (1975) 251, *Cosmological effects of primordial black holes*
- [6] B. J. Carr, Astrophys. J. **201**, 1 (1975), *The Primordial black hole mass spectrum*.
- [7] J. Garcia-Bellido, A. D. Linde and D. Wands, Phys. Rev. D **54**, 6040 (1996) [astro-ph/9605094], “Density perturbations and black hole formation in hybrid inflation.”
- [8] K. Jedamzik and J. C. Niemeyer, Phys. Rev. D **59**, 124014 (1999) [astro-ph/9901293], “Primordial black hole formation during first order phase transitions.”
- [9] P. H. Frampton, M. Kawasaki, F. Takahashi and T. T. Yanagida, JCAP **1004**, 023 (2010) [arXiv:1001.2308 [hep-ph]], *Primordial Black Holes as All Dark Matter*.
- [10] M. Kawasaki, N. Kitajima and T. T. Yanagida, Phys. Rev. D **87**, no. 6, 063519 (2013) [arXiv:1207.2550 [hep-ph]], *Primordial black hole formation from an axionlike curvaton model*.
- [11] K. Kohri, C. M. Lin and T. Matsuda, Phys. Rev. D **87**, no. 10, 103527 (2013) [arXiv:1211.2371 [hep-ph]], *Primordial black holes from the inflating curvaton*.
- [12] G. Chapline and P. H. Frampton, JCAP **1611**, no. 11, 042 (2016) [arXiv:1608.04297 [gr-qc]], *A new direction for dark matter research: intermediate mass compact halo objects*.
- [13] J. M. Ezquiaga, J. Garcia-Bellido, and E. Ruiz Morales, Phys. Lett. B776 (2018) 345–349 arXiv:1705.04861 [astro-ph.CO], “*Primordial Black Hole production in Critical Higgs Inflation*.
- [14] S. Clesse and J. Garcia-Bellido, arXiv:1711.10458 [astro-ph.CO], *Seven Hints for Primordial Black Hole Dark Matter*.
- [15] K. Kohri and T. Terada, arXiv:1802.06785 [astro-ph.CO], *Primordial Black Hole Dark Matter and LIGO/Virgo Merger Rate from Inflation with Running Spectral Indices*.
- [16] Virgo, LIGO Scientific, B. P. Abbott *et al.*, Phys. Rev. Lett. **116**, 061102 (2016), arXiv:1602.03837, *Observation of Gravitational Waves from a Binary Black Hole Merger*.
- [17] VIRGO, LIGO Scientific, B. P. Abbott *et al.*, Phys. Rev. Lett. **118**, 221101 (2017), arXiv:1706.01812, *GW170104: Observation of a 50-Solar-Mass Binary Black Hole Coalescence at Redshift 0.2*.
- [18] M. Sasaki, T. Suyama, T. Tanaka, and S. Yokoyama, Phys. Rev. Lett. **117**, 061101 (2016), arXiv:1603.08338, *Primordial Black Hole Scenario for the Gravitational-Wave Event GW150914*.
- [19] S. Bird *et al.*, Phys. Rev. Lett. **116**, 201301 (2016), arXiv:1603.00464, *Did LIGO detect dark matter?*
- [20] S. Clesse and J. García-Bellido, Phys. Dark Univ. **15**, 142 (2017), arXiv:1603.05234, *The clustering of massive Primordial Black Holes as Dark Matter: measuring their mass distribution with Advanced LIGO*.
- [21] M. Raidal, V. Vaskonen, and H. Veermäe, (2017), arXiv:1707.01480, *Gravitational Waves from Primordial Black Hole Mergers*.

- [22] M. Yu. Khlopov and A. G. Polnarev, Phys. Lett. **97B**, 383 (1980), *PRIMORDIAL BLACK HOLES AS A COSMOLOGICAL TEST OF GRAND UNIFICATION*.
- [23] T. Harada, C.-M. Yoo, K. Kohri, K.-i. Nakao, and S. Jhingan, Astrophys. J. **833**, 61 (2016), arXiv:1609.01588, *Primordial black hole formation in the matter-dominated phase of the Universe*.
- [24] T. Harada, C.-M. Yoo, K. Kohri, and K.-I. Nakao, (2017), arXiv:1707.03595, *Spins of primordial black holes formed in the matter-dominated phase of the Universe*.
- [25] N. Tanahashi and C. M. Yoo, “Spherical Domain Wall Collapse in a Dust Universe,” Class. Quant. Grav. **32**, no. 15, 155003 (2015) [arXiv:1411.7479 [gr-qc]].
- [26] J. Garriga, A. Vilenkin and J. Zhang, “Black holes and the multiverse,” JCAP **1602**, no. 02, 064 (2016) [arXiv:1512.01819 [hep-th]].
- [27] H. Deng, A. Vilenkin and M. Yamada, “CMB spectral distortions from black holes formed by vacuum bubbles,” arXiv:1804.10059 [gr-qc].
- [28] D. K. Nadezhin, I. D. Novikov, and A. G. Polnarev, Soviet Ast. **22**, 129 (1978), *The hydrodynamics of primordial black hole formation*.
- [29] I. D. Novikov and A. G. Polnarev, Soviet Ast. **24**, 147 (1980), *The Hydrodynamics of Primordial Black Hole Formation - Dependence on the Equation of State*.
- [30] M. Shibata and M. Sasaki, Phys. Rev. **D60**, 084002 (1999), arXiv:gr-qc/9905064, *Black hole formation in the Friedmann universe: Formulation and computation in numerical relativity*.
- [31] J. C. Niemeyer and K. Jedamzik, Phys. Rev. **D59**, 124013 (1999), arXiv:astro-ph/9901292, *Dynamics of primordial black hole formation*.
- [32] I. Musco, J. C. Miller, and L. Rezzolla, Class. Quant. Grav. **22**, 1405 (2005), arXiv:gr-qc/0412063, *Computations of primordial black hole formation*.
- [33] A. G. Polnarev and I. Musco, Class. Quant. Grav. **24**, 1405 (2007), arXiv:gr-qc/0605122, *Curvature profiles as initial conditions for primordial black hole formation*.
- [34] I. Musco and J. C. Miller, Class. Quant. Grav. **30**, 145009 (2013), arXiv:1201.2379, *Primordial black hole formation in the early universe: critical behaviour and self-similarity*.
- [35] A. G. Polnarev, T. Nakama, and J. Yokoyama, JCAP **1209**, 027 (2012), arXiv:1204.6601, *Self-consistent initial conditions for primordial black hole formation*.
- [36] T. Nakama, T. Harada, A. G. Polnarev, and J. Yokoyama, JCAP **1401**, 037 (2014), arXiv:1310.3007, *Identifying the most crucial parameters of the initial curvature profile for primordial black hole formation*.
- [37] T. Nakama, JCAP **1410**, 040 (2014), arXiv:1408.0955, *The double formation of primordial black holes*.
- [38] T. Harada, C.-M. Yoo, and K. Kohri, Phys. Rev. **D88**, 084051 (2013), arXiv:1309.4201, *Threshold of primordial black hole formation*, [Erratum: Phys. Rev.D89,no.2,029903(2014)].
- [39] S. Young, C. T. Byrnes, and M. Sasaki, JCAP **1407**, 045 (2014), arXiv:1405.7023, *Calculating the mass fraction of primordial black holes*.
- [40] T. Harada, C.-M. Yoo, T. Nakama, and Y. Koga, Phys. Rev. **D91**, 084057 (2015), arXiv:1503.03934, *Cosmological long-wavelength solutions and primordial black hole formation*.
- [41] M. Kopp, S. Hofmann, and J. Weller, Phys. Rev. **D83**, 124025 (2011), arXiv:1012.4369,

Separate Universes Do Not Constrain Primordial Black Hole Formation.

- [42] J. M. Bardeen, J. R. Bond, N. Kaiser, and A. S. Szalay, *Astrophys. J.* **304**, 15 (1986), *The statistics of peaks of Gaussian random fields*.
- [43] I. Musco (private communication).
- [44] A. G. Doroshkevich, *Astrofizika* **6**, 581 (1970), *The space structure of perturbations and the origin of rotation of galaxies in the theory of fluctuation*.
- [45] K. Ando, K. Inomata, and M. Kawasaki, (2018), arXiv:1802.06393, *Primordial black holes and uncertainties on choice of window function*.